Supporting Information

Integrated Terahertz graphene modulator with 100% modulation depth

Guozhen Liang,[1] Xiaonan Hu,[1] Xuechao Yu,[1] Youde Shen,[4] Lianhe H. Li,[2] Alexander Giles Davies,[2] Edmund H. Linfield,[2] Houkun Liang,[3] Ying Zhang,[3] Qi Jie Wang[1,4,*]

[1] *OPTIMUS, School of Electrical and Electronic Engineering, Nanyang Technological University, 50 Nanyang Avenue, 639798 Singapore.*

[2] *School of Electronic and Electrical Engineering, University of Leeds, Leeds LS2 9JT, UK.*

[3] *Singapore Institute of Manufacturing Technology, Singapore.*

[4] *CDPT, School of Physical and Mathematical Sciences, Nanyang Technological University, 50 Nanyang Avenue, 639798 Singapore.*

**Email: qjwang@ntu.edu.sg*

1. Far field and optical mode of the concentric-circular-grating (CCG) QCL

The design of the concentric-circular grating follows the rule in Ref. 1, with the whole grating structure starting from the center to the boundary being: 59.8/**3**/27.4/**3**/26.3/**3**/26.6/**3**/26.5/**3**/26.4/**3**/27.4/**3**/27.4/**3**/27.4/**3**/27.4/**3**/27.4/**3**/27.4/**3**/27.9/**3**/27.9/**3**/27.9/**3**/27.9/**3**/150 in μm, where the bold numbers indicate the slit region, and the underlined parts are connected by spoke structures to allow electrical pumping of the active region below (Fig. 1 in main text).

The two-dimensional far field emission pattern of the device was measured by scanning a pyroelectric detector on a spherical surface centered at the laser, as shown in Fig. S1a, where the (0, 0) position represents the normal to the laser surface. According to the measured far-field pattern, the optical mode in the laser cavity was identified as that in Fig.S1b and Fig. S1c. As shown, the optical mode is confined in the pumping area (enclosed by a white dash circle) of the CCG QCL. Note that the actual pumped area is

larger than that enclosed by the white dash circle (Fig. S1b) or line (Fig. S1c) since there is lateral current spreading in the active region of typically ~ 20 μm.

From the measured optical mode, it can be deduced that the CCG QCL operates on the sixth-order azimuthal mode[1] although the design was targeted on the first-order mode. This deviation is mainly due to an underestimation of the gain peak frequency of the active region.

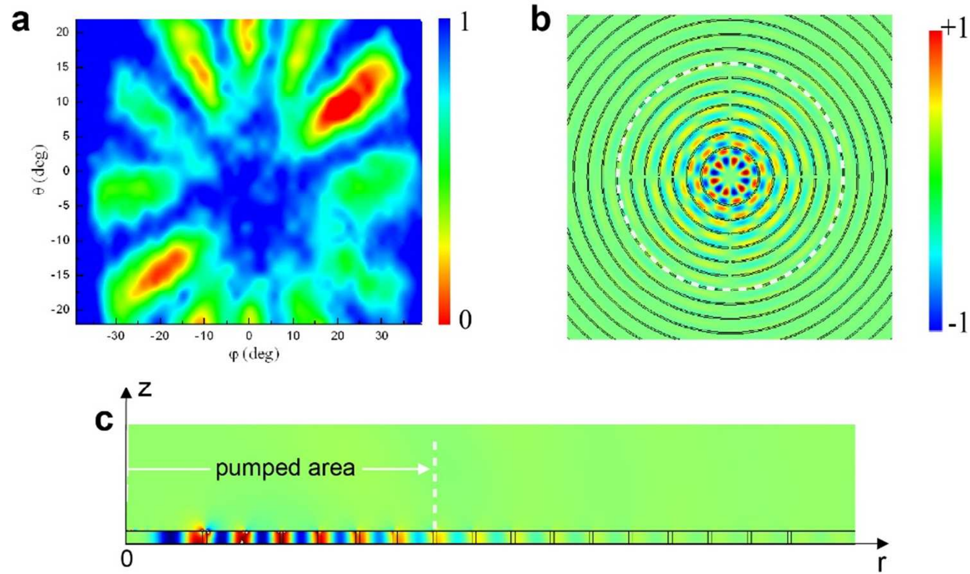

Figure S1. Far field and optical mode of the CCG QCL. a, Measured two-dimensional far-field emission pattern of the surface-emitting CCG QCL, where the (0, 0) position represents the normal to the laser surface. **b** and **c**, Corresponding electric field (E_z) distributions of the laser in plan, and cross-sectional views, respectively. The white dash line illustrates the electrically pumped area.

2. Raman Spectra of the transferrd graphene

Fig. S2a shows the Raman spectrum of the transferred graphene on the SiO_2/Si substrate, and Fig. S2b shows the Raman spectrum of the transferred graphene in different slits (apertures) of the concentric-circular grating of the final device. Compared with Fig. S2a, the additional small peaks in Fig. S2b around

2250cm^{-1} is likely from the chemical residue in the slits. Overall, the near absent D peak, single-Lorentzian-shape 2D peak and the 2D/G intensity ratio (~3) of each spectrum confirm the high quality of the graphene after transfer.

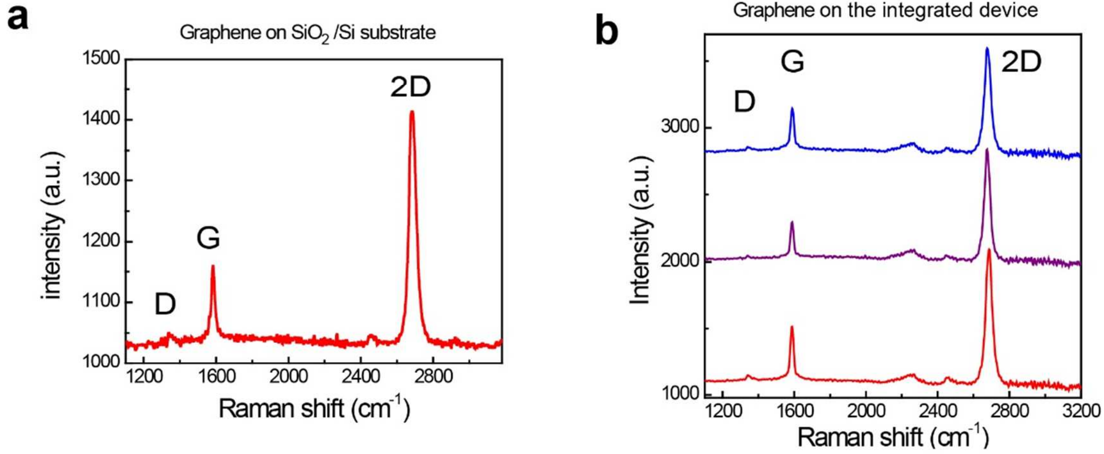

Figure S2. Raman characterization of the transferred graphene. Raman spectra of the transferred graphene on **a**, a SiO_2/p-Si substrate and **b**, in the slits of the CCG of the integrated device.

3. Model used to retrieve the graphene parameters

The carrier density in the graphene can be approximately expressed by:[2]

$$n_{tot} = \sqrt{n_0^2 + n(V_g)^2} \tag{1}$$

Here n_0 represents the residual carrier concentration at the Dirac point, which is non-zero owing to charged impurities in the dielectric or the graphene/dielectric interface.[3] $n(V_g)$ represents the carrier concentration induced by the electric gating, and can be obtained from a parallel capacitor model:

$$V_g - V_{Dir} = \frac{e}{c_{ox}} n + \frac{E_f}{e} \approx \frac{e}{c_{ox}} n \tag{2}$$

$c_{ox} = \varepsilon_0 \varepsilon_{ox} / t$ is the geometrical capacitance, with ε_0 being the permittivity of free space and ε_{ox} the dielectric constant of SiO_2 (~3.9). For oxide thickness of t=450nm, $c_{ox} = 8 \times 10^{-9} F / cm^2$. V_{Dir} is the applied voltage corresponding to the Dirac point.

The square resistance across the source and drain is given by:[2]

$$R_{tot} = R_{contact} + \frac{1}{e n_{tot} u} \quad (3)$$

where $R_{contact}$ represents the metal/graphene contact resistance.

By fitting the measured data with the above model, as shown in Fig. S3, we were able to extract the following parameters: $n_0 = 1.0 \times 10^{12} / cm^2$, $u = 924 cm^2 V^{-1} s^{-1}$, $V_{Dir} = 50.2V$ and $R_{contact} = 440\Omega$.

The graphene sheet conductivity in the main text is given by $1 / \left(R_{tot}(measured) - 440\Omega \right)$, the Fermi level is calculated by $E_f = \hbar \nu_f \sqrt{\pi n_{tot}}$, where $\nu_f \approx 1 \times 10^6 ms^{-1}$ is the Fermi velocity.[4]

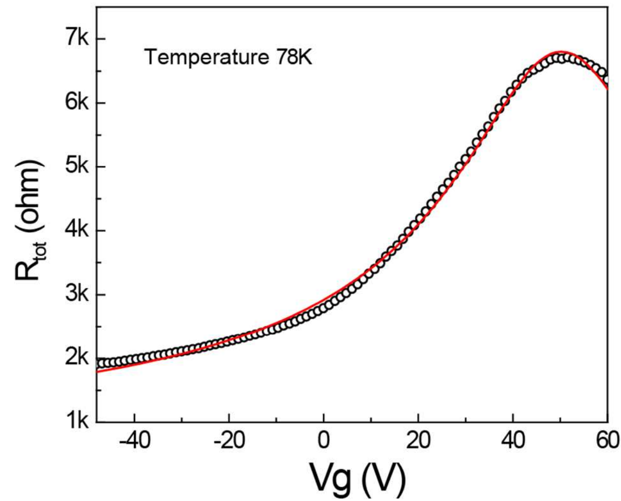

Figure S3. Square resistance of the CVD graphene transistor as a function of gate voltage. The symbols represent measured data, the curve a theoretical fit.

4. Comparison of the graphene response at 78 K and 300 K

To investigate the graphene response at cryogenic and room temperature, we measured the electrical transport and optical modulation of the same graphene sheet at 78 K and 300 K. As plotted in Fig. S4a, at 78 K, the graphene undergoes a larger change of conductivity across the gate voltage range. Treating the graphene as a zero thickness conductive layer with free carriers and current, the transmission intensity at the air/graphene/dielectric interface can be expressed as: [6]

$$\frac{T(\omega, \mathrm{V}_G)}{T(\omega, \mathrm{V}_{Dir})} = \left(\frac{1 + n_{diel} + Z_0 \sigma_0(\omega)}{1 + n_{diel} + Z_0 \sigma(\omega, \mathrm{V}_G)} \right)^2 \tag{4}$$

where n_{diel} is the refractive index of the dielectric, $Z_0 = 376.73\,\Omega$ is the vacuum impedance, $\sigma_0(\omega)$ and $\sigma(\omega, \mathrm{V}_G)$ are the graphene optical conductivity at the Dirac point and V_G gate voltage, respectively. The optical conductivity $\sigma(\omega, \mathrm{V}_G)$ is related to the DC conductivity $\sigma(\mathrm{V}_G)$ measured electrically by $\sigma(\omega, \mathrm{V}_G) = \sigma(\mathrm{V}_G) / \left(1 + \omega^2 \tau^2\right)$, with τ being the carrier momentum scattering time (~15 fs).[4,5] The calculated $T(V_g)/T_{CNP}$ - V_G curves of the THz radiation (at ~3.2 THz) at the air/graphene/SiO_2 interface are also plotted in Fig. S4, showing a slightly higher modulation depth (~1%) at 78 K than that at 300 K. However, the uncertainty in the THz modulation measurement is larger this small difference (Fig. S4b).

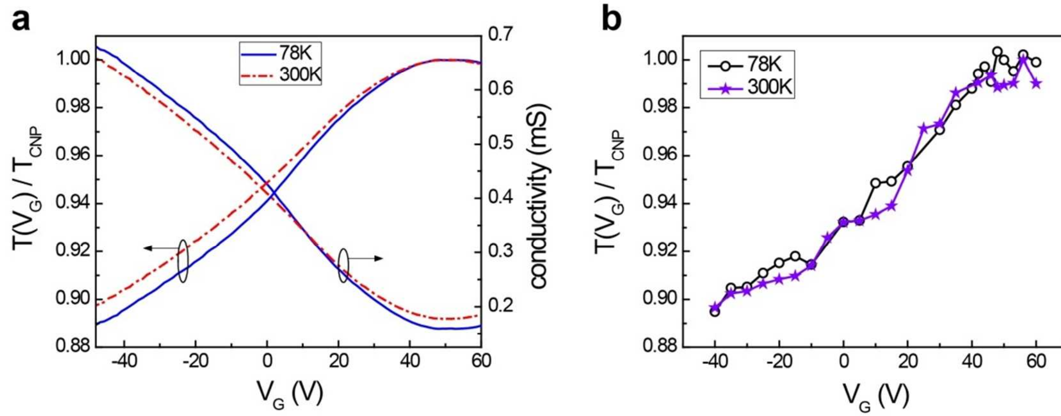

Figure S4. Comparison of the graphene response at 78 K and 300 K. a, Calculated transmittance normalized to the value at the Dirac point and the electrical transport measurements of the graphene sheet at 78 K and 300 K. **b**, Modulation of the THz radiation by the graphene at 78 K and 300 K with the effect of the Si substrate removed. Before removing this substrate effect, the modulation depth is higher (17%).

5. High-frequency circuit model of the graphene modulator

To investigate the high speed performance of the integrated modulator, we constructed an equivalent circuit model. Fig. S5a present the schematic of the modulation scheme, a function generator with output internal impedance R_0 = 50 Ω is placed between the two electrodes that are insulated by the SiO_2 layer. The main components that affect the high frequency performance of the integrated modulator are shown in Fig. S5b, with the cross-section view shown schematically in Fig. S5c. The slits are numbered as 1, 2, 3, ... , . The circuit model for a single slit marked by a dashed box is also shown, where $R^L{}_G$ and $R^R{}_G$ are respectively the resistance of the graphene sheet from the left and right contact edge to the center of the sheet, C_p^L and C_p^R are respectively the capacitance of the left and right contact pads to the back gate, and

C_G is the capacitance between the graphene sheet and the back gate. This circuit can be simplified to that in the lower right model in Fig. S5c, where the parameters can be written as:

$$R_G = \frac{1}{1/R_G^L + 1/R_G^R} \approx \frac{\rho_c + d/2\sigma}{4\pi r} \tag{5}$$

$$C_G = C_p^L + C_p^R = \frac{\varepsilon_{ox}\varepsilon_0(2\pi rd)}{t} \tag{6}$$

Here, ρ_c is the contact resistance across the metal/graphene edge in units of $\Omega \cdot \mu m$, σ is the graphene conductivity, r is the distance from the center of the slit to the center of the device, t is the thickness of the SiO_2 (450 nm), d is the width of the slit (14 μm), ε_0 is the vacuum permittivity and ε_{ox} is the relative permittivity of the SiO_2.

The slits are in parallel in the circuit, and therefore the equivalent circuit for the whole modulator is as shown in Fig. S5d. From the previous two equations, we have

$$\frac{R_G^1}{C_G^1} = \frac{R_G^2}{C_G^2} = \dots = \frac{R_G^6}{C_G^6}. \tag{7}$$

This means the voltages at the red points in Fig. S5d are equal, and we can therefore simplify the circuit model to the one shown in Fig. S5e, where:

$$\begin{aligned} R_G^t &= \frac{1}{1/R_G^1 + 1/R_G^2 + \dots + 1/R_G^6} = \frac{\rho_c + d/2\sigma}{4\pi}\left(\frac{1}{r_1 + r_2 + \dots + r_6}\right) \\ &\approx \frac{\rho_c}{10^4 um} + \frac{2\times 10^{-4}}{\sigma} \\ &\approx 180\,\Omega \end{aligned} \tag{8}$$

$$\begin{aligned} C_G^t &= C_G^1 + C_G^2 + \dots + C_G^6 = \frac{2\pi\varepsilon_{SiO_2}\varepsilon_0 d}{t}(r_1 + r_2 + \dots + r_6) \\ &\approx 6.5\,pF \end{aligned} \tag{9}$$

$$C_p^t = C_p^1 + C_p^2 + \ldots + C_p^6 = \frac{\varepsilon_{SiO_2}\varepsilon_0 A_p}{t} \approx 8.7\,pF \quad (10)$$

A_p is the total area of the graphene contact for slits 1 to 6. In equation (8), $\rho_c = (R_{contact}/2)\times l_{contact} \approx (440\,\Omega/2)\times 8000um$, where $R_{contact}$ is the contact resistance obtained in Section 3, and $l_{contact}$ is the length of the graphene/metal edge of the separated device. Based on the circuit model, the applied gate voltage can be calculated as:

$$V_p = V_S \times \frac{Z_{in}}{Z_{in} + R_0} \quad (11)$$

Where Z_{in} is the total impedance of the modulator, enclosed by the dashed box in Fig. S5e, and can be written as:

$$Z_{in} = \frac{\left[R_G^t + (1/i\omega C_G^t)\right](1/i\omega C_p^t)}{R_G^t + (1/i\omega C_G^t) + (1/i\omega C_p^t)}. \quad (12)$$

Here $\omega = 2\pi f$ with f being the frequency of the modulation signal V_S. The signal that actually drives the carriers in and out of the graphene is

$$V_G = V_S \times \frac{Z_{in}}{Z_{in} + R_0} \times \frac{1}{1 + i\omega R_G^t C_G^t} = V_S \times \frac{1}{1 + i\omega R_0 C_p^t + R_0/(R_G^t + 1/i\omega C_G^t)} \times \frac{1}{1 + i\omega R_G^t C_G^t} \quad (13)$$

To characterize the high-frequency response of the integrated modulator, we have performed an S-parameter measurement using a radio frequency (RF) network analyzer. The dynamic response (S_{21}) is shown in Fig. S6 (blue triangular symbol). The relation between S_{21} and Z_{in} for the circuit in Fig. S5e is:[7]

$$S_{21} = \frac{2Z_{in}}{2Z_{in} + R_0} \tag{14}$$

Combining equations (12) – (14), we get

$$V_G = V_S \times \frac{1}{2/S_{21} - 1} \times \frac{1}{1 + i\omega R_G^t C_G^t} \tag{15}$$

Using the estimated values $R_G^t \approx 180\,\Omega$, and $C_G^t \approx 6.5\,pF$, we are able to plot the normalized modulation depth (V_G/V_S) of the electrical signal applied to the graphene sheet as a function of the modulation frequency (black circular symbol in Fig. S6). The estimated 3-dB cutoff frequency is 110 MHz.

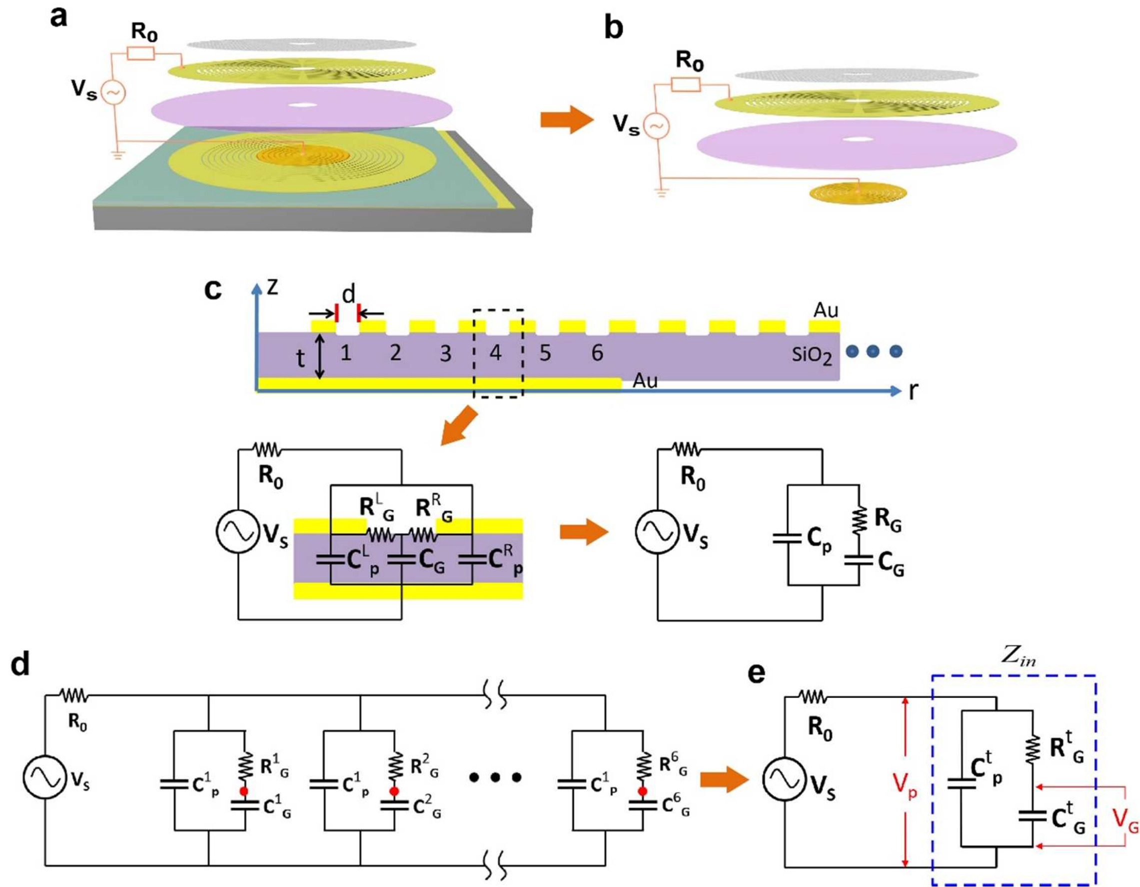

Figure S5. Equivalent circuit model of the integrated graphene modulator. **a**, Schematic of the modulation scheme, the internal impedance of the function generator is R_0 (50 **Ω**). **b**, Principal components that affect the high speed performance of the integrated modulator. **c**, cross-section view of modulator in **b**, and the equivalent circuit for a single slit. **d**, equivalent circuit for the whole modulator. **e**, simplified circuit model for the modulator.

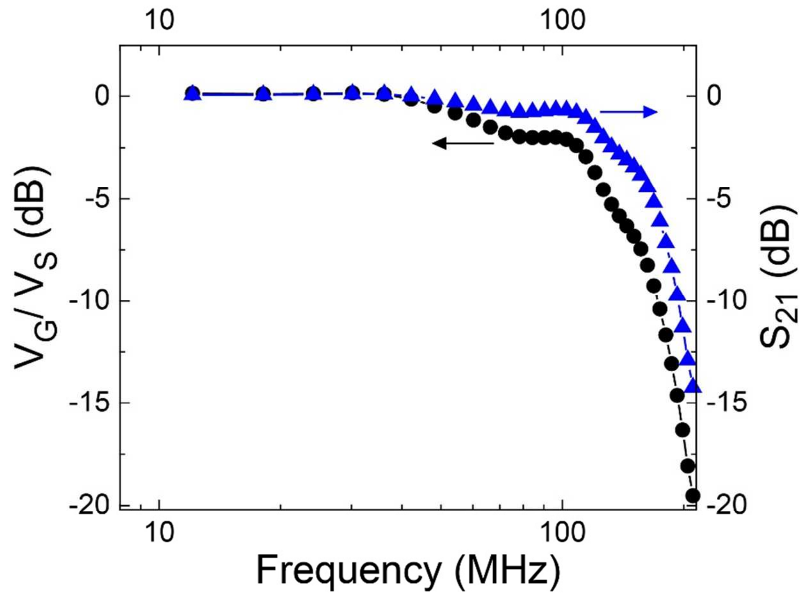

Figure S6. Frequency response of the integrated graphene modulator measured by an RF network analyzer. The blue triangular symbol represents the S_{21} response of the device and the black circular symbol corresponds to the electrical modulation applied to the graphene sheet, with the 3-dB cutoff frequency estimated to be 110 MHz.

Reference

(1) Liang, G.; Liang, H.; Zhang, Y.; Li, L.; Davies, A. G.; Linfield, E.; Yu, S. F.; Liu, H. C.; Wang, Q. J. Low Divergence Single-Mode Surface-Emitting Concentric-Circular-Grating Terahertz Quantum Cascade Lasers. *Opt. Express* **2013**, *21*, 31872.

(2) Kim, S.; Nah, J.; Jo, I.; Shahrjerdi, D.; Colombo, L.; Yao, Z.; Tutuc, E.; Banerjee, S. K. Realization of a High Mobility Dual-Gated Graphene Field-Effect Transistor with Al_2O_3 Dielectric. *Appl. Phys. Lett.* **2009**, *94*, 062107.

(3) Adam, S.; Hwang, E. H.; Galitski, V. M.; Das Sarma, S. A Self-Consistent Theory for Graphene Transport. *Proc. Natl. Acad. Sci. U. S. A.* **2007**, *104*, 18392–18397.

(4) Lee, S. H.; Choi, M.; Kim, T.-T.; Lee, S.; Liu, M.; Yin, X.; Choi, H. K.; Lee, S. S.; Choi, C.-G.; Choi, S.-Y.; Zhang, X.; Min, B. Switching Terahertz Waves with Gate-Controlled Active Graphene Metamaterials. *Nat. Mater.* **2012**, *11*, 936–941.

(5) Valmorra, F.; Scalari, G.; Maissen, C.; Fu, W.; Schönenberger, C.; Choi, J. W.; Park, H. G.; Beck, M.; Faist, J. Low-Bias Active Control of Terahertz Waves by Coupling Large-Area CVD Graphene to a Terahertz Metamaterial. *Nano Lett.* **2013,** *7,* 3193-3198.

(6) Saleh, B. & Teich, M. Fundamentals of Photonics, 2nd edn, Wiley, New York, 2007.

(7) Frickey, D. Conversions between S, Z, Y, H, ABCD, and T Parameters Which Are Valid for Complex Source and Load Impedances. *IEEE Trans. Microw. Theory Tech.* **1994,** *42,* 205–211.